A single-cell atlas of the aging murine ovary

José V. V. Isola[a*], Sarah R. Ocañas[b,c*], Chase R. Hubbart[a], Sunghwan Ko[b], Samim Ali Mondal[a], Jessica D. Hense[a,d], Augusto Schneider[d], Susan Kovats[e], Willard M. Freeman[b,c], Michael B. Stout[a,c]

Institutional Affiliations:
[a]Aging & Metabolism Research Program, Oklahoma Medical Research Foundation, Oklahoma City, OK, USA
[b]Genes & Human Disease Research Program, Oklahoma Medical Research Foundation, Oklahoma City, OK, USA
[c]Oklahoma City Veterans Affairs Medical Center, Oklahoma City, OK, USA
[d]Nutrition College, Federal University of Pelotas, Pelotas, RS, Brazil
[e]Arthritis & Clinical Immunology Research Program, Oklahoma Medical Research Foundation, Oklahoma City, OK, USA

*These authors contributed equally to work presented herein

Email Addresses of Authors:

José V. V. Isola	josevictor-isola@omrf.org
Sarah R. Ocañas	sarah-ocanas@omrf.org
Chase R. Hubbart	chase-hubbart@omrf.org
Sunghwan Ko	sunghwan-ko@ouhsc.edu
Samim Ali Mondal	samim-alimondal@omrf.org
Jessica D. Hense	jessica-hense@omrf.org
Augusto Schneider	augusto.schneider@ufpel.edu.br
Susan Kovats	susan-kovats@omrf.org
Willard M. Freeman	bill-freeman@omrf.org

***Correspondence To:**
Michael B. Stout
Oklahoma Medical Research Foundation
825 NE 13th Street, Chapman S212
Oklahoma City, OK 73104
Phone: 405- 271-1617
Fax: 405-271-1437
michael-stout@omrf.org
ORCID ID: 0000-0002-9996-9123

ABSTRACT

Ovarian aging leads to diminished fertility, dysregulated endocrine signaling, and increased chronic disease burden. These effects begin to emerge long before follicular exhaustion. Around 35 years old, women experience a sharp decline in fertility, corresponding to declines in oocyte quality. However, the field lacks a cellular map of the transcriptomic changes in the aging ovary to identify drivers of ovarian decline. To fill this gap, we performed single-cell RNA sequencing on ovarian tissue from young (3-month-old) and reproductively aged (9-month-old) mice. Our analysis revealed a doubling of immune cells in the aged ovary, with T and B lymphocyte proportions increasing most. We also discovered an age-related upregulation of alternative macrophage and downregulation of collagenase pathways in stromal fibroblasts. Overall, follicular cells (especially granulosa and theca) display stress response, immunogenic, and fibrotic signaling pathway inductions with aging. These changes are more exaggerated in the atretic granulosa cells but are also observed in healthy antral and preantral granulosa cells. Moreover, we did not observe age-related changes in markers of cellular senescence in any cellular population with advancing age, despite specific immune cells expressing senescence-related genes across both timepoints. This report raises several new hypotheses that could be pursued to elucidate mechanisms responsible for ovarian aging phenotypes.

KEYWORDS: collagen, fibrosis, menopause, mouse, multinucleated giant cells, reproduction

INTRODUCTION

Ovarian aging has garnered significant attention in recent years due to a large proportion of women choosing to delay childbearing[1], which causes difficulty with conception and carrying a pregnancy to full-term[2]. As the ovary ages, the local microenvironment changes in ways that reduce oocyte quality and increases the rate of follicular depletion, which eventually results in menopause. Menopause is associated with accelerated systemic aging[3], greater chronic disease burden[4-6], and increased all-cause mortality risk[7]. Therefore, a deeper understanding of the mechanisms that underlie ovarian aging is critically important to extending female fertility and attenuating age-related chronic disease onset.

It is well-established that age-related ovarian follicular depletion is associated with increased mitochondrial dysfunction[8], reactive oxygen species (ROS) production[9,10], inflammation[11-13], and fibrosis[14,15]. However, very little is known about which cell-types develop these phenotypes first and/or dominantly contribute to the changing local microenvironment. Moreover, it remains unclear if cells within the follicle, the stroma, or both play mechanistic roles in promoting follicular depletion and ovarian failure. Recent work has sought to unravel the potential role that ovarian stromal cells play in ovarian health and disease[12,15,16]. We and others have reported that markers of cellular senescence and fibrogenesis increase within the ovarian stroma with aging[11,12,15], although the specific cell-types that become senescent and/or profibrotic remain unknown. In addition to increased senescence and fibrotic markers, the ovarian stroma also accumulates multi-nucleated giant cells (MNGC) with advancing age, which may be related to the mechanisms that promote the aforementioned phenotypes[17].

Due to the complex nature of ovarian function, which change dynamically during aging, it has historically been challenging to elucidate the cell-type-specific mechanisms that promote follicular depletion and ovarian failure. Age-related changes in ovarian transcriptional programs within cellular subtypes remain limited, particularly within mice, which represent the model organism most utilized for ovarian aging studies[18]. Recent advances in single-cell RNA sequencing (scRNA-seq) have expanded our understanding of the diversity of cellular subtypes within various tissues. Herein, we use a scRNA-seq approach to identify age-related transcriptional changes within the murine ovary at 3 and 9 months of age. We chose to analyze 3 and 9 months-old mice because they remain reproductively active at both ages, yet this represents a period where follicular density decreases the most in conjunction with the emergence of age-related hallmarks[11]. This design and approach allowed us to determine how aging modulates cellularity and cellular phenotypes within the ovary prior to overt ovarian failure, which we surmise is viral to developing pharmacological approaches for extending reproductive lifespan in females.

RESULTS

scRNA-seq of the adult murine ovary across reproductive ages

To evaluate age-related changes in the ovarian transcriptional landscape at the single-cell level, we collected ovaries from 3- and 9-month-old female mice (n=4/group). We chose to evaluate the ovaries at these ages because the period from 3 to 9 months represents the time when the greatest decline in follicular reserve occurs and other hallmarks of aging begin to emerge[11], yet the mice remain fertile and reproductively active. Ovaries

were dissociated to create single-cell suspensions, libraries were constructed, and sequencing was performed. Following quality control analyses, filtering, and doublet removal, 14,504 cells remained for characterization. Cellular distributions of the 1) number of detected genes, 2) number of molecules, and 3) proportion of mitochondrial DNA before and after filtering are displayed in Suppl. Fig. 1A. Unbiased clustering and uniform manifold approximation and projection (UMAP) analysis revealed fifteen distinct cellular clusters (CL) (Fig. 1A). One of the CL was present in only one sample and was subsequently identified as oviduct contamination (Suppl. Fig. 1B), therefore these cells were removed from further analyses which left 14349 cells for downstream analyses. To assign cell-type identity, we used cluster-specific markers previously reported in the literature.

Collectively, the largest CL was found to be stromal cells (N=5671), which segregated into three clusters. One of the stromal CL was characterized by having a major *Col1a1* transcriptional signature[19], while another stromal CL was characterized by *Notch3* expression (Fig. 1B), which is classically viewed as a pericyte marker[20,21]. The final stromal CL did not possess any markers that were exclusively expressed within this CL. The second largest CL was found to be the granulosa cells (N=3334) which segregated into two distinct CL, both displaying high expression of *Fshr*[22] (Fig. 1B). This was followed by the theca cell CL (N=1637; *Srd5a1*[23]), two distinct phagocyte CL (N=1099; *C1qa*[24]), endothelial cell CL (N=798; *Cd34*[25]), T-lymphocyte CL (N=728; *Cd3g*[26]), two distinct epithelial cell CL (N=450; *Upk1b*[27] or *Gpm6a*[21]), oocyte CL (N=224; *Zp3*[28]), luteal cell CL (N=206; *Ptgfr*[29]), and B-lymphocyte CL (N=202; *Cd79a*[30]) (Fig. 1B). Feature plots displaying the specificity of these markers to each cluster can be found in Suppl. Fig. 1C.

Advancing age only modestly changed cellularly in the majority of the ovarian cell-types observed in our analyses. However, as expected, granulosa cells were found to be a significantly lower proportion of the total cells in ovaries from 9-month-old mice (Fig. 2A-B), which is supported by the robust decline in follicle numbers in the mice we evaluated (Fig. 2C-D). The most dramatic change in ovarian cellularity between 3- and 9-month-old mice was the greater than 2-fold increase in immune cells (Fig. 2A-B). It is known that ovaries accumulate immune cells during the aging process[13], but to our knowledge, this is the first report to firmly establish this magnitude of change by 9 months of age, when mice remain fertile. It should be noted that estrous cycle staging was not performed in our mice, but the presence of luteal cells in all our samples (Suppl. Fig. 1C) indicates that our mice were in the luteal phase, and not in proestrus or estrus where significant differences in transcriptional signatures are observed[21]. For additional confirmation, we also evaluated the expression of a panel of genes known to change during proestrus and estrus[21], and no consistent differences within groups were observed (Suppl. Fig 1D).

Ovarian immune cell changes with aging

After observing the increased proportion of immune cells within the aged ovarian, we performed further sub-clustering of immune cells to determine which specific cellular populations were changing during the aging process (Fig. 3A) Upon re-clustering, the original immune cell CLs were separated into 13 sub-clusters (SCL) (Fig. 3B). Cell type identification for each SCL was performed with the help of the Cellmarker2.0[31] and ImmGen[32] databases and representative SCL markers were selected (Fig. 3C). Since the overall immune cell proportion doubled from 3 to 9 month of age, percentages of total cells in each SCL were assessed and compared by age.

Intriguingly, the cell-types that showed the greatest increase with age were $CD4^+$ and $CD8^+$ T-Cells, B-cells, and ILC3 Innate Lymphocytes. In contrast, tissue macrophages and monocytes trended towards an increased proportion in the older ovaries, but failed to reach statistical significance (Fig. 3D). One of the macrophage SCLs was only present in the aged ovaries. This SCL was characterized by the expression of CD300e, which negatively regulates T-cell activation[33]. These $CD300e^+$ macrophages might represent a compensatory mechanism to address the T-cell accumulation.

In the aged ovaries, we also observed an increase in *Arg1*$^+$ cells within the monocyte cluster, suggesting that monocyte-derived macrophages in ovary are adopting an alternatively-activated M2 phenotype[34]. Alternative activation of macrophages has also been reported as a stimulus for macrophage fusion and formation of MNGCs[35], which has been reported to be a hallmark of the aging ovary[17]. Although MNGCs were certainly removed from our single-cell suspensions during filtration steps, we were able to observe them in 9-month-old ovaries during histological assessments (Suppl. Fig. 2A). We also noticed that MNGCs accumulate lipofuscin as evidenced by Sudan Black staining (Suppl. Fig. 2A), which has recently been reported as a marker of cellular senescence[36]. Ovarian lipofuscin positivity increased from 3- to 9-months of age (Suppl. Fig. 2B), suggesting that cellular senescence increases within the ovarian with advancing age as we have previously reported[11]. However, it is certainly notable that this increase might be due to an increase in MNGCs rather than an increase in senescent cells. Moreover, given that a greater percentage of immune cells that express senescence-related genes are observed within the ovary during aging (Suppl. Fig. 2C-D), it appears likely that our previously reported increase in ovarian senescence may have been due to increased immune cell infiltration as opposed to greater senescent cell burden.

Sub-clustering of stroma and theca cells reveals age-related phenotypic changes

Several changes in the stroma are observed with ovarian aging and are apparent prior to follicular exhaustion, including cellular senescent signatures[11] and collagen deposition[12,14,15]. To identify potential cellular and molecular mediators of these phenotypes, we performed sub-clustering of the stroma and theca CLs (Fig. 4A). Theca cells (TC) were included since they dynamically differentiate from fibroblastic stromal cells during follicular maturation, and thus, share similarities with stromal cells[36]. This sub-clustering resulted in six distinct SCLs (Fig. 4B). Enriched markers in each SCL were used to infer cell-type-specificity (Fig 4C). The cluster expressing *Inhba*[37,38] identified a subset of granulosa cells (GCs) within the stroma and theca fraction, which could be easily separated at this SCL resolution. The remaining five SCLs were identified as 1) fibroblast-like stromal cells, 2) smooth muscle cells, 3) pericytes, 4) early TC, and 5) TC. Smooth muscle cells were identified by the expression of *Tagln*, *Myh11* and *Actg2*[39]. Pericytes were enriched for *Notch3*, *Rgs5* and *Ebf1*[26]. Fibroblast-like cells had enrichment of *Dcn, Mgp*[40], and *Lum*[19]. Whereas, TCs presented high expression of steroidogenic genes (*Cyp11a1*, *Cyp17a1*[36], and *Mgarp*[26]). The early TC also presented high levels of steroidogenic genes such as *Ptch1* and *Hhip*[41], but also high expression of a fibroblastic gene (*Enpp2*[42]), suggesting that these cells are in transition from stromal fibroblast-like cells to TCs.

After SCL identification, a list of genes differentially expressed by the different ages in each SCL was imported into the IPA software Ingenuity Pathway Analysis (IPA) to infer biological function. Fibroblast-like

stromal cells showed an age-related upregulation of pathways related to tissue remodeling, such as alternative activation of macrophages (Fig. 4D). Tissue remodeling occurs after ovulation and in cases of follicular and luteal atresia[16]. To our surprise, collagen expression was not increased in aged ovarian fibroblast-like cells (Fig. 5A), despite collagen deposition being found to be higher in 9-month-old ovaries through PSR staining (Fig. 5B). Interestingly, collagenase expression was found to be significantly downregulated in fibroblast-like ovarian stroma cells (Fig. 5C), suggesting that collagen accumulation may be due to decreased clearance of collagen. Fibroblast-like cells also experienced downregulated hormonal signaling (estrogen receptor and GNRH) (Fig. 4D), which is somewhat surprising given that hormone levels, estrous cyclicity, and fertility are generally stable at 9 months of age[37]. These results indicate that changes in the local microenvironment may contribute to endocrine dysfunction in the ovarian stroma independent of changes within the follicle. In contrast to the fibroblast-like cells, TCs showed a significant upregulation in several upstream regulators of fibrogenesis including TGFB1, TGFB2, and SMAD3 (Fig. 5C), which suggests TC may be one of the earliest cell-types involved in generating the signaling cascade for collagen production and deposition. TCs also displayed a modest age-related upregulation in inflammation and cell stress response pathways (Fig. 5E), which were mirrored by upstream regulators involved in cellular proliferation including MTOR, YAP1, and RB1 (Fig. 5D).

Sub-clustering of granulosa, oocytes and luteal cells reveal age-related proinflammatory changes

Cellular populations of GC, oocytes, and luteal cells were sub-clustered into 6 distinct SCLs (Fig. 6A-C). GCs were further segregated into four distinct SCL that were identified as being part of follicles that were in different stages of development. The SCL included preantral, antral, mitotic, and atretic GCs. GCs signal to oocytes to provide cues related to the local ovarian microenvironment, in addition to converting androgens to estrogens which are released into the systemic circulation or feedback signaling in the brain[38]. GCs from immature follicles that have not yet developed an antrum are referred to as preantral GCs and were identified by enrichment in *Igfbp5*[39] and *Gatm*[40] expression. GCs from antral follicles (antral GCs) were identified by enrichment of *Inhbb*[41,42]. A separate GC SCL, which we refer to as mitotic GCs, as expressed *Inhbb* similarly to antral GCs, but displayed enriched expression of cell division markers *Top2a*[43] and *Racgap1*[44]. Lastly, GCs from follicles undergoing atresia were found to have enriched expression of *Cald1*[45], *Pik31p1*[46], and *Itih5*[21]. Oocytes were easily identified by the expression of classical markers *Gdf9*, *Ooep* and *Zp3*[28]. Luteal cells, which consist of remnant GCs and TCs following ovulation and constitute the corpus luteum[47], were identified by the expression of *Ptgfr*[29].

As alluded to above, differentially expressed genes from each SCL were imported into IPA software to infer biological function. Interestingly, preantral, antral, and atretic GCs all displayed an age-related increases in pathways related to proinflammatory stress and fibrogenesis (Fig. D-F). These observations corresponded to a significant increase in the mitochondrial dysfunction pathway within oocytes (Fig. 6G). Upstream regulators related to proinflammatory stress that were found to be increased in GC SCL included IFNG, TNF, IL15, and IL1a (Fig. 6H). Additionally, upstream regulators related to fibrogenesis that were found to be increased in GC SCL included TGFB1, Tgf beta, and SMAD3 (Fig. 6H). As expected, the atretic GC SCL displayed the greatest degree of increase in regulators of proinflammatory stress and fibrosis, although it should be noted that older

animals (9 months) displayed much greater phenotypes when compared to young mice (3 months). Therefore, it appears that aging exacerbates inflammatory and fibrotic responses that are required for ovarian remodeling following ovulation and follicular atresia. Lastly, upstream regulators linked to the alternative activation of immune cells, IL4 and IL13, were also found to be upregulated in GC SCLs, which may play a role in the formation of MNGCs as alluded to above.

Sub-clustering of endothelial and epithelial cells reveals only minor age-related changes

Endothelial cells constitute the blood and lymphatic vessels. The ovary is a highly vascularized organ with blood vessels that travel through connective tissue to assist with hormone & nutrient trafficking and waste removal[48]. The ovary has a rich lymphatic network closely associated with the blood vasculature that is involved in immune cell trafficking[49]. Epithelial cells comprise the ovarian surface, facilitate repair following ovulation, and dynamically expand and contract during cyclic ovarian changes[50]. In addition, epithelium cells share a common progenitor with granulosa cells[51]. Endothelium and epithelium CLs were sub-clustered together (Fig. 7A) and resulted in four distinct SCLs (Fig. 7B). Vascular and lymphatic endothelium were separated and identified by the enrichment of specific cellular markers (Fig. 7C). Vascular endothelial cells showed enrichment of *Flt1*[52] and *Mmrn2*[53], whereas lymphatic endothelial cells were enriched for *Lyve1*[54] expression. Similar to findings in the stroma/theca SCLs, one of the epithelium/endothelium SCLs was found to be enriched for GC markers and was removed from further analyses. No age differences were observed in this GC SCL. The only epithelium/endothelium SCL that displayed age-related changes in the pathway analyses was the vascular endothelium. This SCL was found to have a modest increase DNA damage regulation (Fig. 7D). Another interesting observation was that upstream regulators of cellular senescence (Tp53, Cdkn1a, and Cdkn2a) were found to be increased with aging in vascular endothelial cells (Fig. 7E). A further analysis of genes that are downstream of Tp53, Cdkn1a, and Cdkn2a were found to be altered in directionality consistent with the activation of these upstream regulators (Fig. 7F). However, gene expression of *Tp53, Cdkn1a,* and *Cdkn2a* did not change in advancing age within the vascular endothelial SCL (Fig. 7G). At this juncture it remains unclear if ovarian vascular endothelial cells become senescent beyond 9 months of age.

DISCUSSION

In this report, we assessed age-related changes in murine ovarian transcriptome at single-cell resolution. During aging, ovarian follicular reserve declines, and there is concomitant deterioration of the ovarian microenvironment as evidenced by increased inflammation and fibrosis. Importantly, these changes occur prior to follicular exhaustion[11] and likely contribute to decreased oocyte quality and diminished reproductive success until the onset of menopause. However, specific cellular contributions to ovarian aging phenotypes are not yet elucidated, limiting the development of interventional approaches to extend female fertility. Whole ovarian transcriptomic assessments can provide misleading results due to potential changes in cell heterogeneity that occur during aging. Cell sorting can overcome this limitation but may require pooling multiple murine ovaries to obtain sufficient cells for downstream analyses and relies on specific antibodies or cre-reporter systems to target specific cell-types. scRNA-seq, on the other hand, is a useful tool to simultaneously measure transcriptomic

changes of all ovarian cell types during the aging process. Previous ovarian scRNA-seq have identified the molecular signatures of specific cell-types and changes in individual cell populations[21,28,40,55-57]. In mice, estrous-cycle[21] and primordial follicle assembly[55] result in dynamic changes in specific ovarian cellular populations. However, the specific cellular changes occurring during ovarian aging are still being elucidated, especially with regards to the critical period of diminished fertility that occurs long before follicular exhaustion. Since mice are the primary model organisms used for ovarian aging experiments[18], the single-cell ovarian aging atlas generated here serve as a crucial resource for the field. In non-human primates, scRNA-seq provided mechanistic insights into changes associated with ovarian aging[28]. However, this study was conducted with animals in the peri-menopausal state[58], when alterations in cyclicity and hormone levels are perturbed. Our primary goal was to identify early changes that occur in reproductively aged mice prior to the peri-estropausal period. At 9 months of age, mice experience declined ovarian reserve[11], but remain fertile[59], modeling a critical age when women seek to have children and experience difficulty conceiving[2]. A marked increase in embryonic aneuploidy is observed in embryos from women starting around the age of 35[60], suggesting loss of oocyte quality at this age. With our approach, we differentiated all of the main cell-types expected in the ovaries and further subdivided them to determine specific cellular populations altered by the aging process.

Our results show that, at 9 months of age, the proportion of immune cells is already doubled in the ovaries. The immune cell types that increase the most in the aged ovaries are B cells, T cells, and innate lymphoid cells. B cells and $CD4^+$ T cell accumulation has been previously reported in the aged ovary[13], however these changes were not identified prior to 12 months of age. Chronic ovarian inflammation caused by autoimmune disease also leads to lymphocyte infiltration[61] and women with autoimmune diseases often experience ovarian insufficiency[62]. This suggests that accumulating immune cells might contribute to age-related follicular decline. The accumulation of T cells in the aged ovaries might also be a response to a repeated need for tissue remodeling, since these cells are involved in tissue healing[63]. However, different types of T cells play various roles in tissue remodeling, and T cell responses can also contribute to the pathogenesis of fibrosis[63]. We detected a distinct macrophage cluster that was only present in the aged ovaries and was positive for Cd300e expression. CD300e is associated with negative regulation of T cell activation[33], which suggests the emergence of these macrophages might be a compensatory mechanism to dampen T cell accumulation. Alternatively activated macrophages can also suppress T-cells accumulation[64]. We observed an increase in *Arg1*$^+$ cells in the monocytes SCL, which likely represents alternative activation of these cells into M2 macrophages. An increase in alternatively activated macrophages has previously been reported in aged ovaries[34] and is believed to contribute to collagen deposition in the ECM[65]. M2 macrophages are involved in collagen fibril assembly and fibrogenesis[66]. Alternative activation pathways are also associated with macrophage fusion, which is known to generate MNGCs. MNGCs are a hallmark of the aging ovary[35]. Here, we detected ovarian MNGCs at 9 months of age, which is the earliest observation of these structures, to our knowledge. MNGCs efficiently engulf large particles *in vitro*[67]. In the ovaries, phagocytic processes are essential for debris removal following follicular atresia, corpus luteum regression, and ovulation. With aging, however, MNGC formation and function may serve a pathogenic role by contributing to fibrosis and inflammation[17]. Additionally, the presence of MNGCs in the post-reproductive ovary could contribute to systemic inflammation and aging phenotypes. MNGCs have also been

associated with redox-active iron accumulation, may promote oxidative stress[68], and also accumulate lipofuscin. Hence, measurements of Sudan Black staining in the aging ovary likely marks MNGC accumulation as opposed to cellular senescence. Additionally, most immune cell types in the ovary were found to be positive for senescence markers, even the ovaries from young animals. Thus, previous bulk sequencing analyses that detected increased senescence in aged ovaries were likely detecting the increased immune cell abundance.

Fibrosis and collagen accumulation in the ECM are also hallmarks of ovarian aging[12,14,15]. Within the fibroblast-like stroma SCL, we observed enhancement in alternative activation of macrophages pathways with aging, suggesting that fibroblastic tissue remodeling might also contribute to the formation of MNGCs. Fibroblast-like stromal cells showed upregulated IL12 pathway in the aged ovary, which can contribute to naïve $CD4^+$ T cell activation into Th1 cells[69]. Th1 cells are known to be pro-fibrotic[63]. In alignment with prior studies, we observed increased collagen deposition in the aged ovaries, although here we report it at a younger age than previously reported[12,14,15]. Since collagen is believed to be produced by the stromal fibroblast cells, we looked at the expression of collagen genes in this SCL, but observed no changes with advancing age. Conversely, , collagenase processes were downregulated in the aged ovaries, suggesting that collagen accumulation might occur due to dysregulated clearance. In turn, diminished fibroblast function may also lead to alternative macrophage activation and T-cell recruitment[63,65].

Similar to fibroblasts, TC showed upregulated IL12 and alternative macrophage activation pathways, albeit to a lesser extent. In TC, we also observed an increase in genes associated with cell proliferation, such as mTOR, YAP1, and RB1, which are also altered with aging[70]. mTOR signaling is also intimately involved in follicular progression. Upregulation of mTOR promotes the activation of primordial follicles, which expedites ovarian reserve depletion[71]. Hence, the upregulation of mTOR in TC may affect local environment thereby activating primordial follicles and contributing to the exhaustion of ovarian reserve. Age-related changes in GC are similar to those observed in TC, although the phenotypes are more severe. Oxidative phosphorylation, endoplasmic reticulum stress, and IL8 signaling were upregulated in TCs and GCs with advancing age, as well as pro-inflammatory and fibrotic regulators, including TGFβ. Atretic GC, which are GC from follicles undergoing atresia, showed a marked enhancement in pro-inflammatory upstream regulators, as well oxidative stress and fibrosis. Since this comparison is performed with GC undergoing atresia in both ages, the upregulation of pro-inflammatory and cellular stress pathways and regulators suggests that aging exacerbates the response to follicular atresia. Intriguingly, antral and preantral GC from follicles not undergoing atresia also had an upregulation of cellular stress, pro-inflammation signaling, and fibrosis pathways in the aging ovary. Pro-inflammation and fibrosis upstream regulators were also enriched in these cells, mainly in the antral GC, although less than in the atretic GC. Besides the classical pro-inflammatory regulators, atretic GC also had increased IL4 and IL13 with aging, which triggers alternative activation of immune cells. Overall, aged follicular cells present an exacerbated response to environmental stressors which likely contributes to chronic inflammation. Thus, we hypothesize that early inflammatory and pro-fibrotic changes in the stroma and follicular cells lead to immune expansion and infiltration which enhances the inflammatory ovarian microenvironment and could also be associated with enhanced mitochondrial dysfunction in the oocytes.

As for senescence markers, little differences were observed between 3- and 9-month-old ovaries. These results could be explained by the nature of single-cell analysis, in which we subdivide the cellular populations to assess individual changes, which affects the sensitivity of analyses. Also, 9-month-old mice might be considered too young to observe dramatic changes in cellular senescence, although prior studies have reported increased transcriptional marker of cellular senescence by 9 months of age[11]. However, we demonstrate in the current report that ovarian immune cells express numerous senescence-related genes regardless of age, therefore the age-related increase in ovarian senescence markers may be just mirroring the expansion of immune cell populations. Vascular endothelial cells, however, did show increased cellular senescence upstream regulators. However, these changes might also measure altered cell cycle and be due to possible changes in blood flow in the aged ovaries, as the actual expression of the senescence marker genes was not changed in these cells. Further exploration of senescence in older ovaries is still warranted.

In summary, this report if the first provide insight into changes that occur within the aging mouse ovary with single-cell resolution. We show that by 9 months of age, when mice remain fertile and reproductively active, immune cell infiltration is already more than doubled, with the largest changes being observed in T and B lymphocytes. We also demonstrate that GC and TC induce stress response, immunogenic, and fibrotic signaling pathways with aging, whereas fibroblast-like stroma cells increase alternative activation of macrophage pathways. These changes were mirrored by increased accumulation of MNGCs with advancing age, which were also found to contain the majority of lipofuscin staining in aging ovaries. This observation, coupled with the increase in immune cells that are known to commonly express transcriptional markers of cellular senescence, like contribute to the previously reported increase in ovarian cellular senescence with advancing age. Collectively, our findings provide insight into the underlying mechanisms that promote chronic ovarian inflammation and fibrosis with advancing age and raise several new hypotheses that could be pursued in order to better understand ovarian aging.

METHODS

Animals and tissue collection and dissociation: All animal procedures were approved by the Institutional Animal Care and Use Committee at the Oklahoma Medical Research Foundation (OMRF). C57BL/6J (Strain# 000664) female mice (N=8) were purchased from the Jackson Laboratory (Bar Harbor, ME) and acclimated to the OMRF animal facility before ovary collection. At 3 (n=4) or 9 months of age (n=4), mice were anesthetized with isoflurane and euthanized by exsanguination due to cardiac puncture. Perfusion was performed with 1X PBS, and ovaries were collected and dissected. One ovary from each mouse was dissociated using a Multi Tissue Dissociation Kit 1 (cat# 130110201, Miltenyi Biotec), following manufacturer's instructions to create a single-cell suspension in D-PBS (cat# 14287080, Gibco).

scRNA-Seq library construction: scRNA-Seq libraries were constructed with the Chromium Single Cell 3' GEM, Library & Gel Bead Kit v3 (cat# 10000075, 10X Genomics), according to the manufacturer's instructions as briefly described below. Following the creation of ovarian single-cell suspensions, cells were counted on the

MACSQuant10 flow cytometer and diluted to 1000 cells per microliter to target the recovery of 5000 cells per sample during scRNA-seq encapsulation. The diluted cells, master mix, gel beads, and partitioning oil were added to the Chromium Single Cell B Chip (cat# 10000073, 10X Genomics) and loaded into the Chromium controller (cat#1000204, 10X Genomics) to generate the gel beads-in-emulsion (GEMs) for downstream library preparation. GEMs were then transferred to PCR strip tubes and incubated in a thermocycler to perform reverse transcription in GEMs (GEM-RT). Following GEM-RT, the recovery agent was aspirated, and cDNA was cleaned using the Dynabeads MyOne SILANE reagent included in the scRNA-seq kit. The cDNA was amplified and then cleaned using SPRISelect reagent beads (cat#B23318, Beckman Coulter). The cDNA was quality checked using a High Sensitivity D5000 ScreenTape (cat#5067- 5592, Agilent) run on a TapeStation 2200 (cat#G2964AA, Agilent). An aliquot of 25% of amplified cDNA was carried forward to library preparation. Libraries were quantified by qPCR and quality checked on a High Sensitivity D1000 ScreenTape (cat# 5067- 5584, Agilent) on the TapeStation 2220. Libraries were normalized, pooled, and sequenced on the NovaSeq6000 PE150 flow cell.

scRNA-Seq Quality control and data analysis: Fastq files were generated and demultiplexed from raw base call (bcl) files using the cellranger mkfastq pipeline. Alignment, filtering, barcode counting, and UMI counting were conducted using the cellranger count pipeline using the refdata-gex-mm10-2020-A reference transcriptome with default settings. The resultant out files were loaded into R using the “load10X” function of the SoupX package[72]. The SoupX pipeline was then used to estimate and remove ambient RNA contamination before converting to Seurat objects[73]. Samples were then merged to create a single Seurat object and filtered based on the number of features (>200) and percent mitochondrial transcripts (<25%). Genes that were expressed in less than three cells were removed from analysis. Genes that represent ribosomal contamination (*Malat1, Gm42418, Gm26917, Ay036118*)[74,75] were causing technical background noises and were removed from the analysis to improve subclustering. Variable features were identified in Seurat before scaling data and running PCA. The JackStraw method was used to determine the dimensionality of the dataset, and a UMAP analysis was generated in Seurat. Doublets were identified and removed using the DoubletFinder package[76] with 5% doublets expected. Other parameters (pN=0.25, pK=0.01) were generated using the DoubletFinder sweep statistics. Samples were co-projected on a UMAP which was used to determine that there were no batch effects and that further data integration was not necessary. Seurat was used to find differentially expressed genes by cluster and age and to generate plots presented in the figures (i.e., DimPlot, VlnPlot, DotPlot). Gene lists were imported into the IPA software Ingenuity Pathway Analysis (IPA) 01.12 (Qiagen Bioinformatics) to assess pathway/biological function enrichment analysis.

Histology: The remaining ovary from each mouse was collected into 4% PFA, processed, and serially sectioned. To determine ovarian reserve, one of every six serial sections from the whole ovary was H&E stained and follicles from each state were counted as described previously[77]. The number of preantral follicles (primordial, primary, secondary) were multiplied by six to account for sections that were not evaluated and then multiplied by two to account for both ovaries. Due to their large size, antral follicles were multiplied by three to account for sections that were not evaluated and then multiplied by two to account for both ovaries. Picro-Sirius Red staining for

collagen deposition and Sudan Black staining for lipofuscin accumulation were performed as previously described[11,12].

Statistics: Differentially expressed genes (DEGs) between clusters and by age were called in the Seurat package, using the FindMarkers command with default parameters. DEG lists were imported into IPA software and filtered on FDR<0.1 and logFC>0.25 for pathway analyses. Pathways with p<0.05 were considered statistically significant and the activation z-scores were reported by heatmap or bar charts in the figures. More traditional statistical analyses were done using GraphPad Prism software. Strip plots are presented with individual points shown and means ± SEM indicated. For comparisons of means between the two ages, Student's t-test's were used, applying one- and two-tailed tests as appropriate. Corrections for multiple comparisons were made, where appropriate, using the Benjamini, Krieger, and Yekutieli correction for multiple comparisons. Significant differences were defined at P<0.05 or FDR<0.05 (for multiple comparisons).

ACKNOWLEDGEMENTS

This work was supported by the National Institutes of Health (R01 AG069742 to M.B.S.) and Presbyterian Health Foundation (Pilot Research Funding to M.B.S.). The authors thank the staff at the Clinical Genomics Center and Imaging Core Facility at the Oklahoma Medical Research Foundation for assistance with sequencing and histological procedures.

AUTHOR CONTRIBUTIONS

J.V.V.I., S.R.O., and M.B.S. conceived the project and designed the experiments. J.V.V.I. and S.R.O. performed the experiments and data analyses with contributions from C.R.H., S.K., S.A.M., J.D.H., A.S., S.K., and W.M.F. J.V.V.I., S.R.O., and C.R.H. created figures and performed statistical analyses with contributions from W.M.F. and M.B.S. J.V.V.I., S.R.O., and M.B.S. wrote the manuscript and all authors edited and approved the final draft.

DATA AVAILABILITY STATEMENT

The datasets generated through this work are available upon reasonable request from the corresponding author.

COMPLETING INTERESTS

The authors declare no conflicts or competing interests.

REFERENCES

1 Johnson, J. A. & Tough, S. No-271-Delayed Child-Bearing. *J Obstet Gynaecol Can* **39**, e500-e515, doi:10.1016/j.jogc.2017.09.007 (2017).

2 Broekmans, F. J., Soules, M. R. & Fauser, B. C. Ovarian aging: mechanisms and clinical consequences. *Endocr Rev* **30**, 465-493, doi:10.1210/er.2009-0006 (2009).

3 Levine, M. E. *et al.* Menopause accelerates biological aging. *Proc Natl Acad Sci U S A* **113**, 9327-9332, doi:10.1073/pnas.1604558113 (2016).

4 Wellons, M., Ouyang, P., Schreiner, P. J., Herrington, D. M. & Vaidya, D. Early menopause predicts future coronary heart disease and stroke: the Multi-Ethnic Study of Atherosclerosis. *Menopause* **19**, 1081-1087, doi:10.1097/gme.0b013e3182517bd0 (2012).

5 Tchernof, A., Calles-Escandon, J., Sites, C. K. & Poehlman, E. T. Menopause, central body fatness, and insulin resistance: effects of hormone-replacement therapy. *Coron Artery Dis* **9**, 503-511, doi:10.1097/00019501-199809080-00006 (1998).

6 Muka, T. *et al.* Association of Age at Onset of Menopause and Time Since Onset of Menopause With Cardiovascular Outcomes, Intermediate Vascular Traits, and All-Cause Mortality: A Systematic Review and Meta-analysis. *JAMA Cardiol* **1**, 767-776, doi:10.1001/jamacardio.2016.2415 (2016).

7 Ossewaarde, M. E. *et al.* Age at menopause, cause-specific mortality and total life expectancy. *Epidemiology* **16**, 556-562, doi:10.1097/01.ede.0000165392.35273.d4 (2005).

8 May-Panloup, P. *et al.* Ovarian ageing: the role of mitochondria in oocytes and follicles. *Hum Reprod Update* **22**, 725-743, doi:10.1093/humupd/dmw028 (2016).

9 Lim, J. & Luderer, U. Oxidative damage increases and antioxidant gene expression decreases with aging in the mouse ovary. *Biol Reprod* **84**, 775-782, doi:10.1095/biolreprod.110.088583 (2011).

10 Yang, L. *et al.* The Role of Oxidative Stress and Natural Antioxidants in Ovarian Aging. *Front Pharmacol* **11**, 617843, doi:10.3389/fphar.2020.617843 (2020).

11 Ansere, V. A. *et al.* Cellular hallmarks of aging emerge in the ovary prior to primordial follicle depletion. *Mech Ageing Dev* **194**, 111425, doi:10.1016/j.mad.2020.111425 (2021).

12 Briley, S. M. *et al.* Reproductive age-associated fibrosis in the stroma of the mammalian ovary. *Reproduction* **152**, 245-260, doi:10.1530/REP-16-0129 (2016).

13 Lliberos, C. *et al.* Evaluation of inflammation and follicle depletion during ovarian ageing in mice. *Sci Rep* **11**, 278, doi:10.1038/s41598-020-79488-4 (2021).

14 Amargant, F. *et al.* Ovarian stiffness increases with age in the mammalian ovary and depends on collagen and hyaluronan matrices. *Aging Cell* **19**, e13259, doi:10.1111/acel.13259 (2020).

15 Umehara, T. *et al.* Female reproductive life span is extended by targeted removal of fibrotic collagen from the mouse ovary. *Sci Adv* **8**, eabn4564, doi:10.1126/sciadv.abn4564 (2022).

16 Mara, J. N. *et al.* Ovulation and ovarian wound healing are impaired with advanced reproductive age. *Aging (Albany NY)* **12**, 9686-9713, doi:10.18632/aging.103237 (2020).

17 Foley, K. G., Pritchard, M. T. & Duncan, F. E. Macrophage-derived multinucleated giant cells: hallmarks of the aging ovary. *Reproduction* **161**, V5-V9, doi:10.1530/REP-20-0489 (2021).

18 Lu, H. *et al.* Current Animal Model Systems for Ovarian Aging Research. *Aging Dis* **13**, 1183-1195, doi:10.14336/AD.2021.1209 (2022).

19 Muhl, L. *et al.* Single-cell analysis uncovers fibroblast heterogeneity and criteria for fibroblast and mural cell identification and discrimination. *Nat Commun* **11**, 3953, doi:10.1038/s41467-020-17740-1 (2020).

20 Baek, S. H. *et al.* Single Cell Transcriptomic Analysis Reveals Organ Specific Pericyte Markers and Identities. *Front Cardiovasc Med* **9**, 876591, doi:10.3389/fcvm.2022.876591 (2022).

21 Morris, M. E. *et al.* A single-cell atlas of the cycling murine ovary. *Elife* **11**, doi:10.7554/eLife.77239 (2022).

22 Li, S. *et al.* Single-cell RNA sequencing analysis of mouse follicular somatic cellsdagger. *Biol Reprod* **105**, 1234-1245, doi:10.1093/biolre/ioab163 (2021).

23 Marti, N. *et al.* Genes and proteins of the alternative steroid backdoor pathway for dihydrotestosterone synthesis are expressed in the human ovary and seem enhanced in the polycystic ovary syndrome. *Mol Cell Endocrinol* **441**, 116-123, doi:10.1016/j.mce.2016.07.029 (2017).

24 Sontheimer, R. D., Racila, E. & Racila, D. M. C1q: its functions within the innate and adaptive immune responses and its role in lupus autoimmunity. *J Invest Dermatol* **125**, 14-23, doi:10.1111/j.0022-202X.2005.23673.x (2005).

25 Lin, G., Finger, E. & Gutierrez-Ramos, J. C. Expression of CD34 in endothelial cells, hematopoietic progenitors and nervous cells in fetal and adult mouse tissues. *Eur J Immunol* **25**, 1508-1516, doi:10.1002/eji.1830250606 (1995).

26 Garcillan, B. *et al.* CD3G or CD3D Knockdown in Mature, but Not Immature, T Lymphocytes Similarly Cripples the Human TCRalphabeta Complex. *Front Cell Dev Biol* **9**, 608490, doi:10.3389/fcell.2021.608490 (2021).

27 Carpenter, A. R. *et al.* Uroplakin 1b is critical in urinary tract development and urothelial differentiation and homeostasis. *Kidney Int* **89**, 612-624, doi:10.1016/j.kint.2015.11.017 (2016).

28 Wang, S. *et al.* Single-Cell Transcriptomic Atlas of Primate Ovarian Aging. *Cell* **180**, 585-600 e519, doi:10.1016/j.cell.2020.01.009 (2020).

29 Berisha, B., Rodler, D., Schams, D., Sinowatz, F. & Pfaffl, M. W. Prostaglandins in Superovulation Induced Bovine Follicles During the Preovulatory Period and Early Corpus Luteum. *Front Endocrinol (Lausanne)* **10**, 467, doi:10.3389/fendo.2019.00467 (2019).

30 Chu, P. G. & Arber, D. A. CD79: a review. *Appl Immunohistochem Mol Morphol* **9**, 97-106, doi:10.1097/00129039-200106000-00001 (2001).

31 Hu, C. *et al.* CellMarker 2.0: an updated database of manually curated cell markers in human/mouse and web tools based on scRNA-seq data. *Nucleic Acids Res* **51**, D870-D876, doi:10.1093/nar/gkac947 (2023).

32 Heng, T. S., Painter, M. W. & Immunological Genome Project, C. The Immunological Genome Project: networks of gene expression in immune cells. *Nat Immunol* **9**, 1091-1094, doi:10.1038/ni1008-1091 (2008).

33 Coletta, S. *et al.* The immune receptor CD300e negatively regulates T cell activation by impairing the STAT1-dependent antigen presentation. *Sci Rep* **10**, 16501, doi:10.1038/s41598-020-73552-9 (2020).

34 Zhang, Z., Schlamp, F., Huang, L., Clark, H. & Brayboy, L. Inflammaging is associated with shifted macrophage ontogeny and polarization in the aging mouse ovary. *Reproduction* **159**, 325-337, doi:10.1530/REP-19-0330 (2020).

35 Martinez, F. O., Helming, L. & Gordon, S. Alternative activation of macrophages: an immunologic functional perspective. *Annu Rev Immunol* **27**, 451-483, doi:10.1146/annurev.immunol.021908.132532 (2009).

36 Evangelou, K. & Gorgoulis, V. G. Sudan Black B, The Specific Histochemical Stain for Lipofuscin: A Novel Method to Detect Senescent Cells. *Methods Mol Biol* **1534**, 111-119, doi:10.1007/978-1-4939-6670-7_10 (2017).

37 Nelson, J. F., Felicio, L. S., Randall, P. K., Sims, C. & Finch, C. E. A longitudinal study of estrous cyclicity in aging C57BL/6J mice: I. Cycle frequency, length and vaginal cytology. *Biol Reprod* **27**, 327-339, doi:10.1095/biolreprod27.2.327 (1982).

38 Dompe, C. *et al.* Human Granulosa Cells-Stemness Properties, Molecular Cross-Talk and Follicular Angiogenesis. *Cells* **10**, doi:10.3390/cells10061396 (2021).

39 Meinsohn, M. C. *et al.* Single-cell sequencing reveals suppressive transcriptional programs regulated by MIS/AMH in neonatal ovaries. *Proc Natl Acad Sci U S A* **118**, doi:10.1073/pnas.2100920118 (2021).

40 Fan, X. *et al.* Single-cell reconstruction of follicular remodeling in the human adult ovary. *Nat Commun* **10**, 3164, doi:10.1038/s41467-019-11036-9 (2019).

41 Chen, A. Q., Wang, Z. G., Xu, Z. R., Yu, S. D. & Yang, Z. G. Analysis of gene expression in granulosa cells of ovine antral growing follicles using suppressive subtractive hybridization. *Anim Reprod Sci* **115**, 39-48, doi:10.1016/j.anireprosci.2008.10.022 (2009).

42 Wigglesworth, K., Lee, K. B., Emori, C., Sugiura, K. & Eppig, J. J. Transcriptomic diversification of developing cumulus and mural granulosa cells in mouse ovarian follicles. *Biol Reprod* **92**, 23, doi:10.1095/biolreprod.114.121756 (2015).

43 Lee, J. H. & Berger, J. M. Cell Cycle-Dependent Control and Roles of DNA Topoisomerase II. *Genes (Basel)* **10**, doi:10.3390/genes10110859 (2019).

44 Blanchard, J. M. Cyclin A2 transcriptional regulation: modulation of cell cycle control at the G1/S transition by peripheral cues. *Biochem Pharmacol* **60**, 1179-1184, doi:10.1016/s0006-2952(00)00384-1 (2000).

45 Hatzirodos, N., Irving-Rodgers, H. F., Hummitzsch, K. & Rodgers, R. J. Transcriptome profiling of the theca interna from bovine ovarian follicles during atresia. *PLoS One* **9**, e99706, doi:10.1371/journal.pone.0099706 (2014).

46 Piersanti, R. L., Santos, J. E. P., Sheldon, I. M. & Bromfield, J. J. Lipopolysaccharide and tumor necrosis factor-alpha alter gene expression of oocytes and cumulus cells during bovine in vitro maturation. *Mol Reprod Dev* **86**, 1909-1920, doi:10.1002/mrd.23288 (2019).

47 Stocco, C., Telleria, C. & Gibori, G. The molecular control of corpus luteum formation, function, and regression. *Endocr Rev* **28**, 117-149, doi:10.1210/er.2006-0022 (2007).

48 Brown, H. M. & Russell, D. L. Blood and lymphatic vasculature in the ovary: development, function and disease. *Hum Reprod Update* **20**, 29-39, doi:10.1093/humupd/dmt049 (2014).

49 Brown, H. M., Robker, R. L. & Russell, D. L. Development and hormonal regulation of the ovarian lymphatic vasculature. *Endocrinology* **151**, 5446-5455, doi:10.1210/en.2010-0629 (2010).

50 Hartanti, M. D. *et al.* Formation of the Bovine Ovarian Surface Epithelium during Fetal Development. *J Histochem Cytochem* **68**, 113-126, doi:10.1369/0022155419896797 (2020).

51 Hummitzsch, K. *et al.* A new model of development of the mammalian ovary and follicles. *PLoS One* **8**, e55578, doi:10.1371/journal.pone.0055578 (2013).

52 Schulz, A. *et al.* The Soluble Fms-like Tyrosine Kinase-1 Contributes to Structural and Functional Changes in Endothelial Cells in Chronic Kidney Disease. *Int J Mol Sci* **23**, doi:10.3390/ijms232416059 (2022).

53 Galvagni, F. *et al.* Dissecting the CD93-Multimerin 2 interaction involved in cell adhesion and migration of the activated endothelium. *Matrix Biol* **64**, 112-127, doi:10.1016/j.matbio.2017.08.003 (2017).

54 Fujimoto, N. *et al.* Single-cell mapping reveals new markers and functions of lymphatic endothelial cells in lymph nodes. *PLoS Biol* **18**, e3000704, doi:10.1371/journal.pbio.3000704 (2020).

55 Wang, J. J. *et al.* Single-cell transcriptome landscape of ovarian cells during primordial follicle assembly in mice. *PLoS Biol* **18**, e3001025, doi:10.1371/journal.pbio.3001025 (2020).

56 Wagner, M. *et al.* Single-cell analysis of human ovarian cortex identifies distinct cell populations but no oogonial stem cells. *Nat Commun* **11**, 1147, doi:10.1038/s41467-020-14936-3 (2020).

57 Pei, J. *et al.* Single-Cell Transcriptomics Analysis Reveals a Cell Atlas and Cell Communication in Yak Ovary. *Int J Mol Sci* **24**, doi:10.3390/ijms24031839 (2023).

58 Gilardi, K. V., Shideler, S. E., Valverde, C. R., Roberts, J. A. & Lasley, B. L. Characterization of the onset of menopause in the rhesus macaque. *Biol Reprod* **57**, 335-340, doi:10.1095/biolreprod57.2.335 (1997).

59 Isola, J. V. V. *et al.* Mild calorie restriction, but not 17alpha-estradiol, extends ovarian reserve and fertility in female mice. *Exp Gerontol* **159**, 111669, doi:10.1016/j.exger.2021.111669 (2022).

60 Franasiak, J. M. *et al.* The nature of aneuploidy with increasing age of the female partner: a review of 15,169 consecutive trophectoderm biopsies evaluated with comprehensive chromosomal screening. *Fertil Steril* **101**, 656-663 e651, doi:10.1016/j.fertnstert.2013.11.004 (2014).

61 Dong, Y. *et al.* The role of regulatory T cells in thymectomy-induced autoimmune ovarian disease. *Am J Reprod Immunol* **78**, doi:10.1111/aji.12683 (2017).

62 Sharif, K. *et al.* Insights into the autoimmune aspect of premature ovarian insufficiency. *Best Pract Res Clin Endocrinol Metab* **33**, 101323, doi:10.1016/j.beem.2019.101323 (2019).

63 Zhang, M. & Zhang, S. T Cells in Fibrosis and Fibrotic Diseases. *Front Immunol* **11**, 1142, doi:10.3389/fimmu.2020.01142 (2020).

64 Huber, S., Hoffmann, R., Muskens, F. & Voehringer, D. Alternatively activated macrophages inhibit T-cell proliferation by Stat6-dependent expression of PD-L2. *Blood* **116**, 3311-3320, doi:10.1182/blood-2010-02-271981 (2010).

65 Wynn, T. A. & Vannella, K. M. Macrophages in Tissue Repair, Regeneration, and Fibrosis. *Immunity* **44**, 450-462, doi:10.1016/j.immuni.2016.02.015 (2016).

66 Knipper, J. A. *et al.* Interleukin-4 Receptor alpha Signaling in Myeloid Cells Controls Collagen Fibril Assembly in Skin Repair. *Immunity* **43**, 803-816, doi:10.1016/j.immuni.2015.09.005 (2015).

67 Milde, R. *et al.* Multinucleated Giant Cells Are Specialized for Complement-Mediated Phagocytosis and Large Target Destruction. *Cell Rep* **13**, 1937-1948, doi:10.1016/j.celrep.2015.10.065 (2015).

68 Asano, Y. Age-related accumulation of non-heme ferric and ferrous iron in mouse ovarian stroma visualized by sensitive non-heme iron histochemistry. *J Histochem Cytochem* **60**, 229-242, doi:10.1369/0022155411431734 (2012).

69 Trinchieri, G. Interleukin-12 and the regulation of innate resistance and adaptive immunity. *Nat Rev Immunol* **3**, 133-146, doi:10.1038/nri1001 (2003).

70 Liu, G. Y. & Sabatini, D. M. mTOR at the nexus of nutrition, growth, ageing and disease. *Nat Rev Mol Cell Biol* **21**, 183-203, doi:10.1038/s41580-019-0199-y (2020).

71 Schneider, A. *et al.* The Interconnections Between Somatic and Ovarian Aging in Murine Models. *J Gerontol A Biol Sci Med Sci* **76**, 1579-1586, doi:10.1093/gerona/glaa258 (2021).

72 Young, M. D. & Behjati, S. SoupX removes ambient RNA contamination from droplet-based single-cell RNA sequencing data. *Gigascience* **9**, doi:10.1093/gigascience/giaa151 (2020).

73 Satija, R., Farrell, J. A., Gennert, D., Schier, A. F. & Regev, A. Spatial reconstruction of single-cell gene expression data. *Nat Biotechnol* **33**, 495-502, doi:10.1038/nbt.3192 (2015).

74 Liu, Y. *et al.* Single-Cell Profiling Reveals Divergent, Globally Patterned Immune Responses in Murine Skin Inflammation. *iScience* **23**, 101582, doi:10.1016/j.isci.2020.101582 (2020).

75 Nguyen, H. T. T., Guevarra, R. B., Magez, S. & Radwanska, M. Single-cell transcriptome profiling and the use of AID deficient mice reveal that B cell activation combined with antibody class switch recombination and somatic hypermutation do not benefit the control of experimental trypanosomosis. *PLoS Pathog* **17**, e1010026, doi:10.1371/journal.ppat.1010026 (2021).

76 McGinnis, C. S., Murrow, L. M. & Gartner, Z. J. DoubletFinder: Doublet Detection in Single-Cell RNA Sequencing Data Using Artificial Nearest Neighbors. *Cell Syst* **8**, 329-337 e324, doi:10.1016/j.cels.2019.03.003 (2019).

77 Isola, J. V. V. *et al.* 17alpha-Estradiol promotes ovarian aging in growth hormone receptor knockout mice, but not wild-type littermates. *Exp Gerontol* **129**, 110769, doi:10.1016/j.exger.2019.110769 (2020).

FIGURES & FIGURE LEGENDS

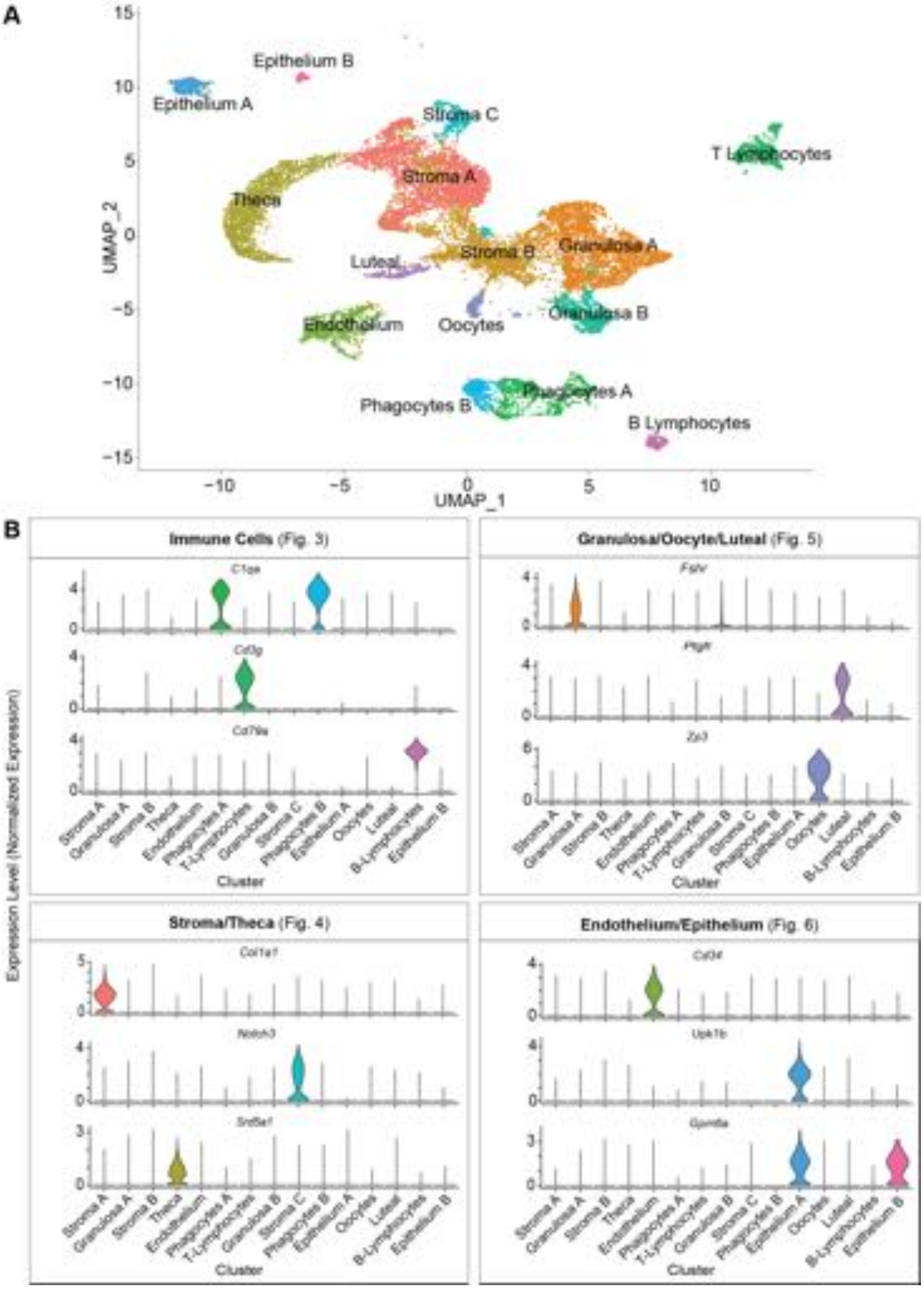

Fig. 1. scRNA-seq of the murine ovary. Whole ovarian tissue was collected from 3- and 9-month-old C57BL/6J mice and processed for 10X Genomics 3' scRNA-Seq. (A) UMAP plot of age-combined ovarian cells. Clustering analysis revealed 15 distinct ovarian cell populations. (B) Violin plots of specific marker genes for each ovarian cell type.

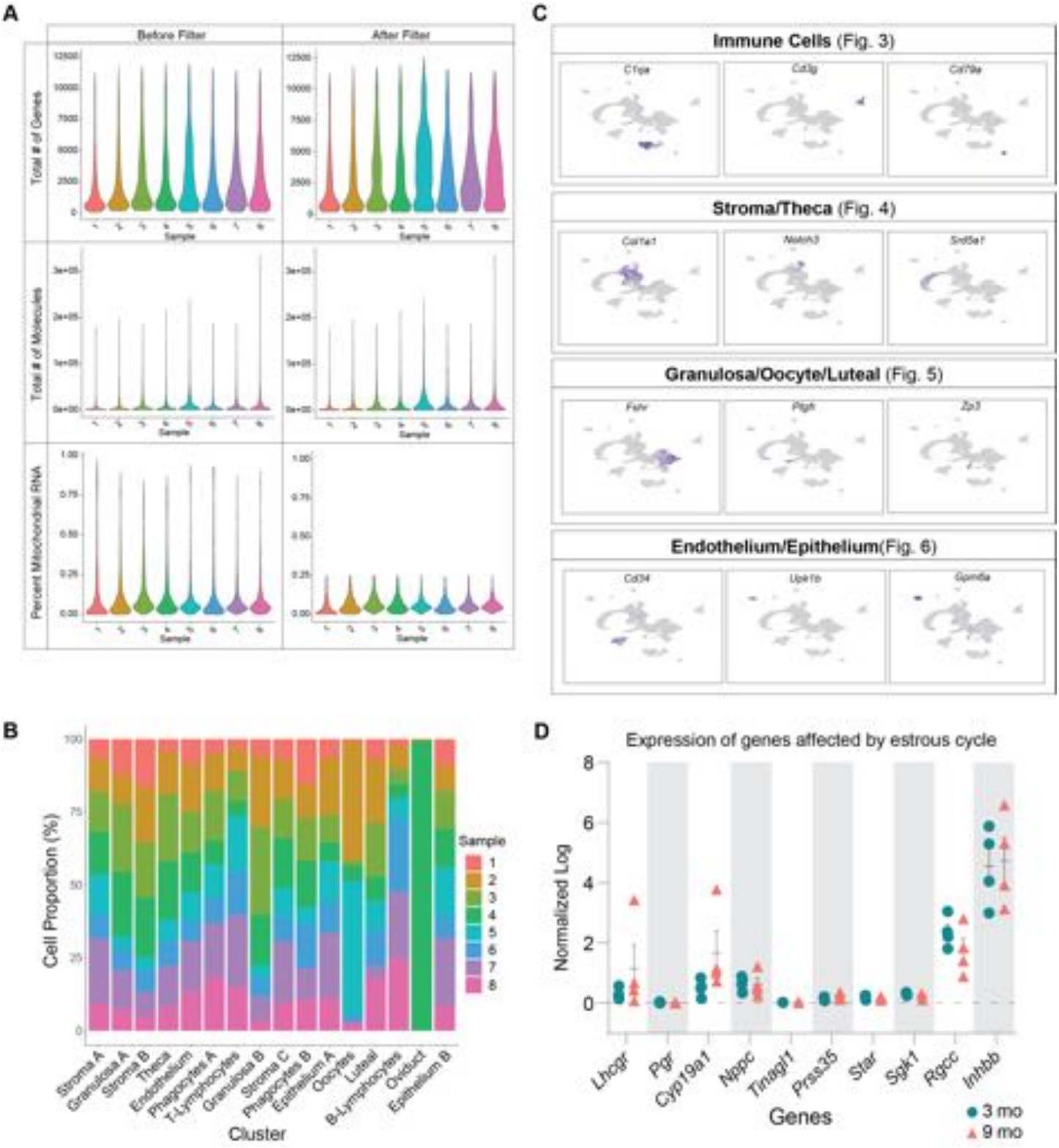

Suppl. Fig. 1. (A) Violin plots of the total number of genes and molecules and mitochondrial percentages within each sample before and after quality filtering. (B) Feature plots of specific marker genes of cell types used to identify the clusters. (C) Percentage of cells in each cluster by sample, showing oviduct cells contamination in one sample which was removed from further analyses. (D) Expression of genes reported to be affected by estrous cycle stages in granulosa cells.

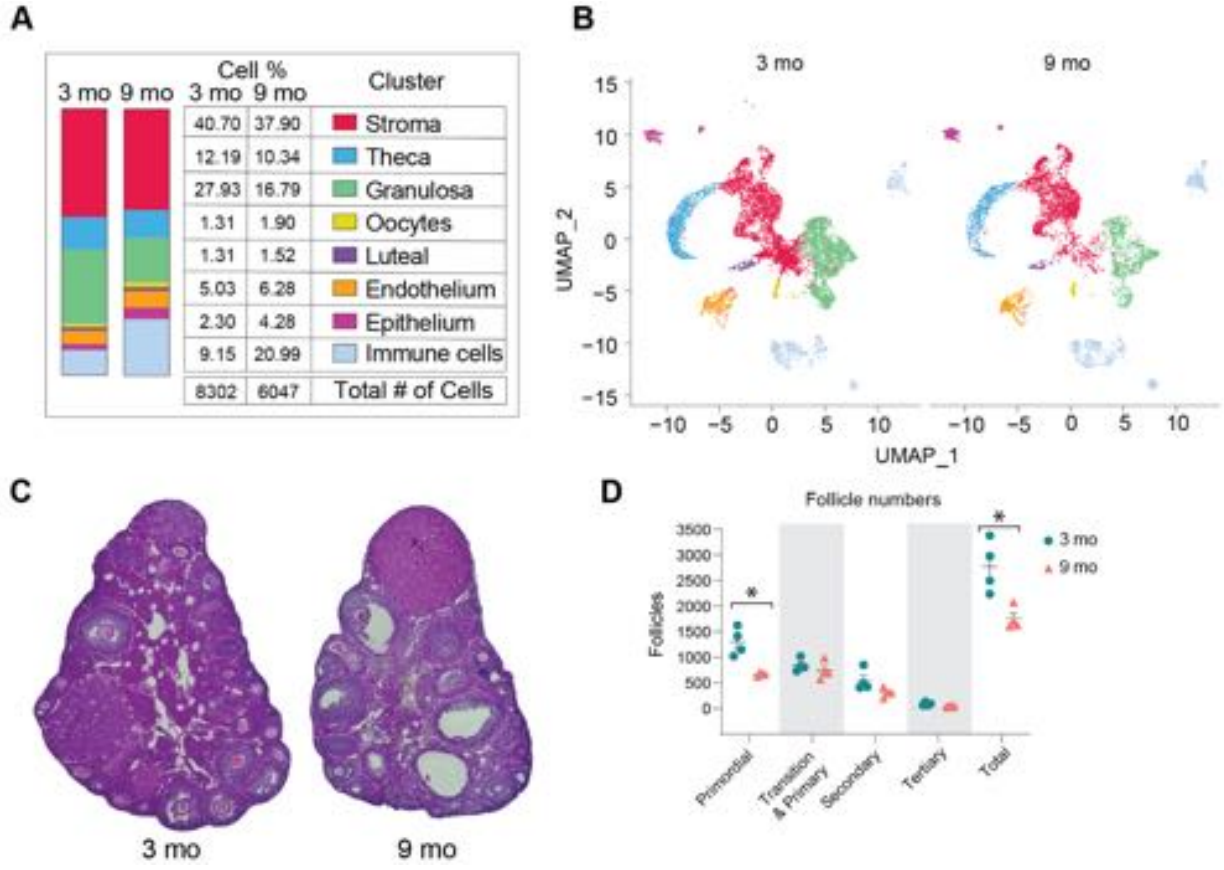

Fig. 2. Age-related changes in ovarian cell populations. (A) The number and percentage of cells in broad categories of cell type identity by age. (B) UMAP plot of ovarian cells split by age. (C) Representative images of H&E stained ovaries. (D) Estimated number of ovarian follicles in 3- and 9-month-old ovaries. Data are presented as mean ± SEM. * represents statistical difference ($p<0.05$) by two-tailed t-test.

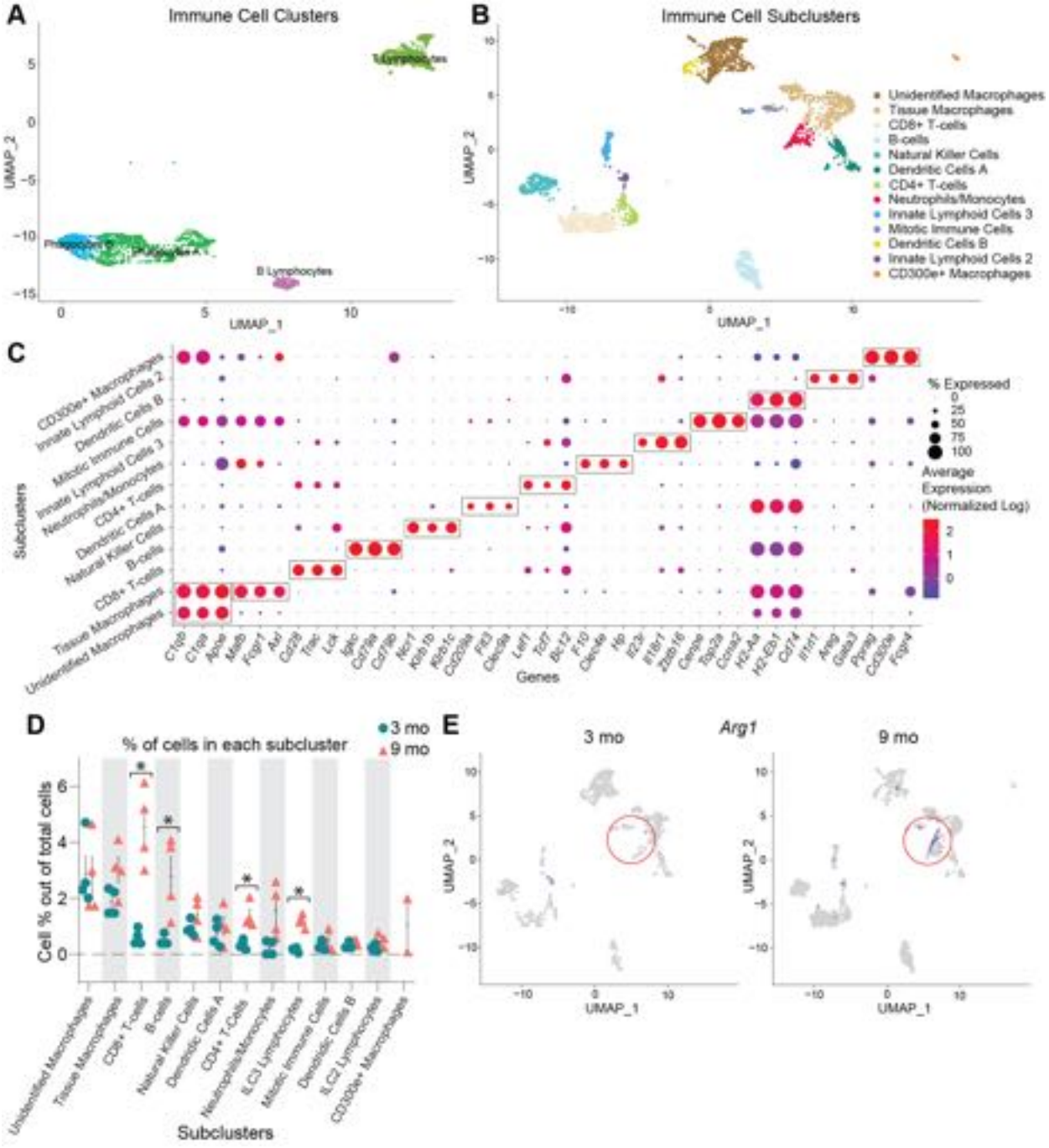

Fig. 3. Immune cells accumulate in the ovaries with age. (A) UMAP of immune clusters selected for sub-clustering analyses. (B) UMAP of immune sub-clusters. (C) Dot plot of markers used for SCL cell-type identification. (D) Percentage of cells in each immune SCL out of total cells. (E) Feature plot of *Arg1* expression. Data are presented as mean ± SEM. * represents statistical difference (FDR<0.05) by multiple two-tailed t-test with Benjamini, Krieger, and Yekutieli correction for multiple comparisons.

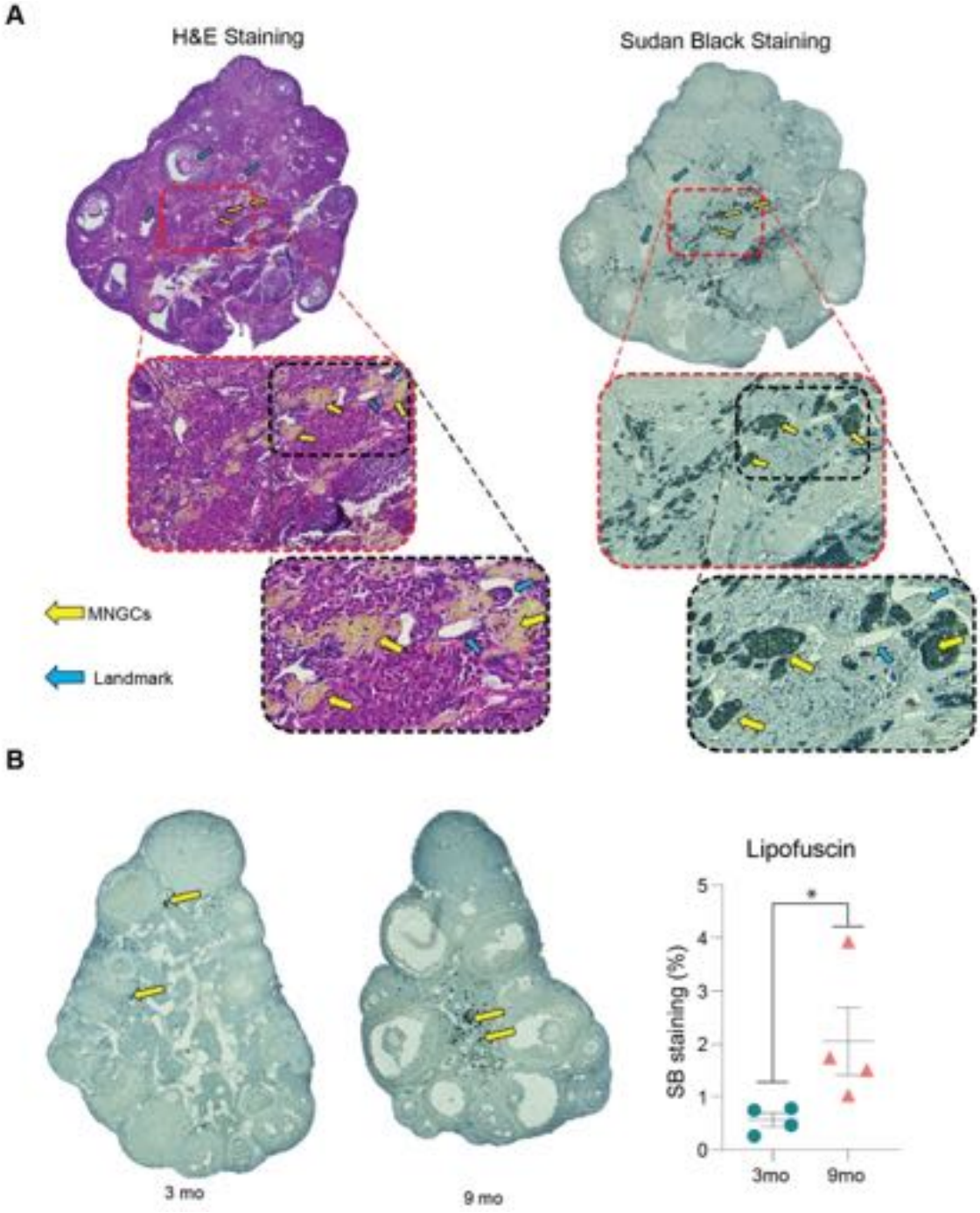

Suppl. Fig. 2. Assessment of lipofuscin accumulation in the aged ovary. (A) H&E and Sudan black staining of 9-month-old ovarian sections showing MNGC accumulation compared to 3-month-old ovaries. (B) Sudan black staining of lipofuscin in 3- and 9-month-old ovaries. Data are presented as mean ± SEM. * represents statistical difference ($p<0.05$) by one-tailed t-test.

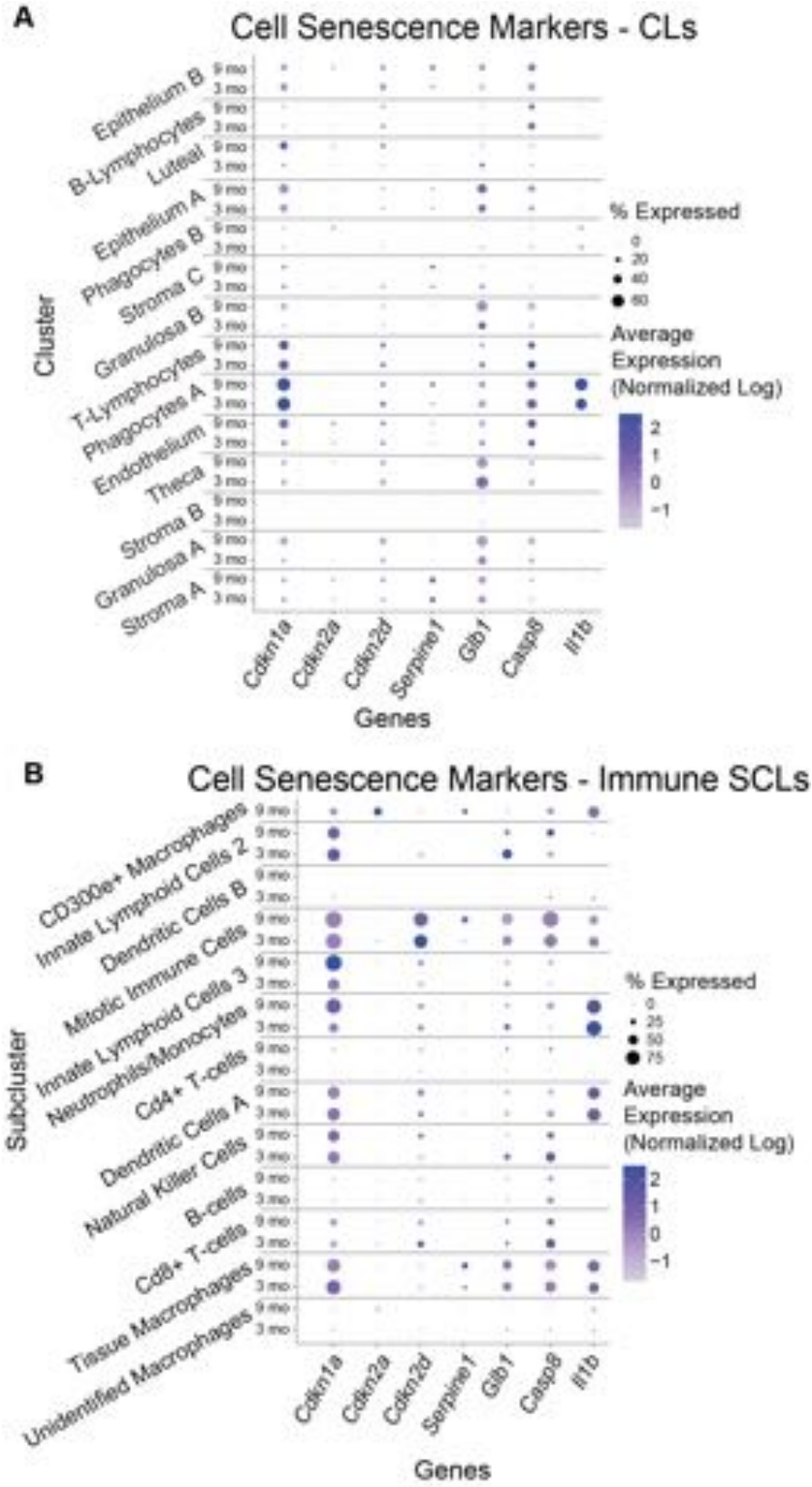

Suppl. Fig. 3. Expression of cellular senescence markers is unchanged with age. (A) Dot plot of expression of cellular senescence markers in initial CLs. (B) Dot plot of expression of cell senescence markers in immune SCLs.

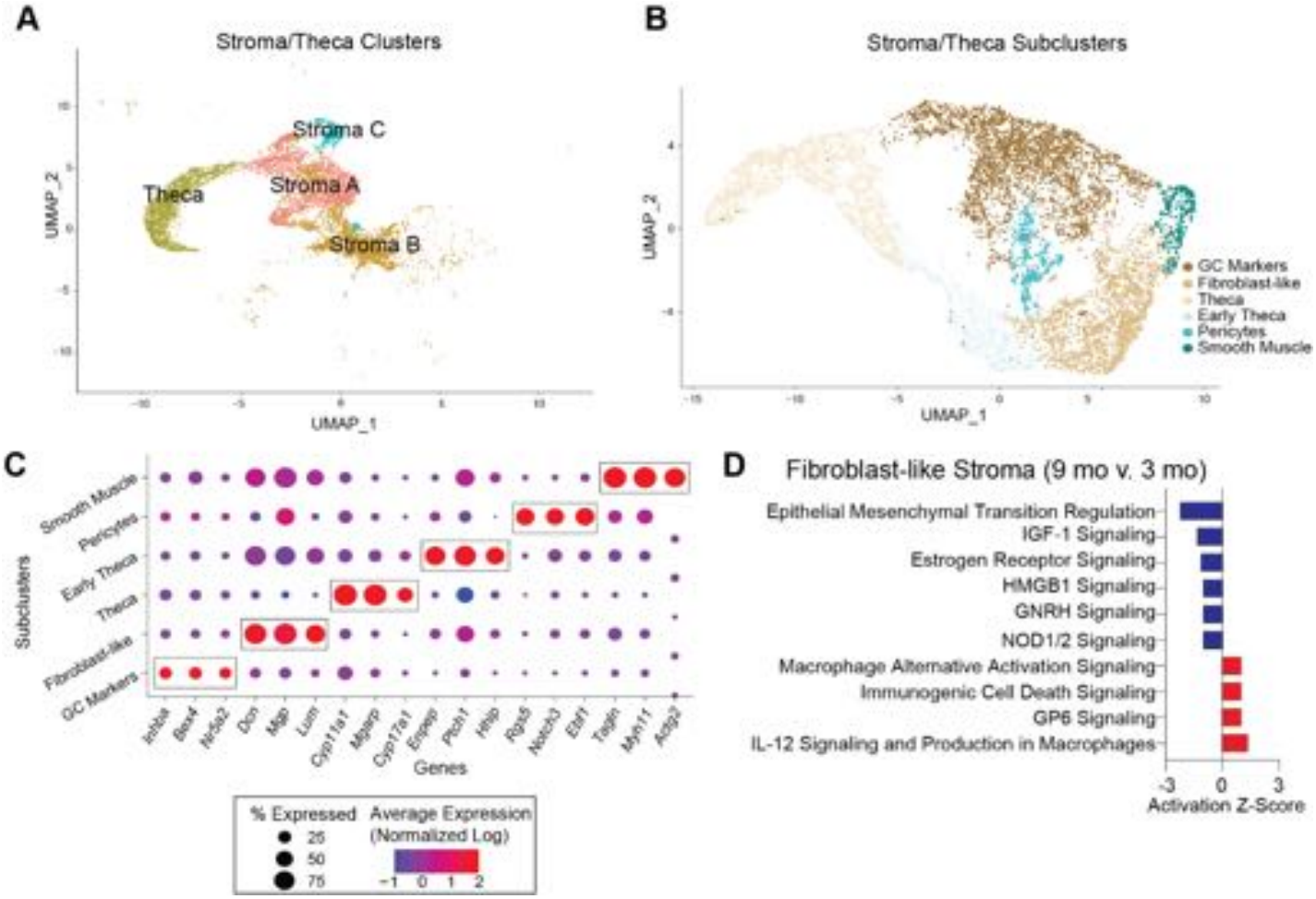

Fig. 4. Sub-clustering of stroma and theca cells. (A) UMAP of stroma and theca CLs used for sub-clustering (B) UMAP of stroma and theca SCLs. (C) Dot plot of markers used for SCL cell-type identification. (D) IPA canonical pathways indicating activation or inhibition of specific pathways by aging in stromal fibroblast-like cells.

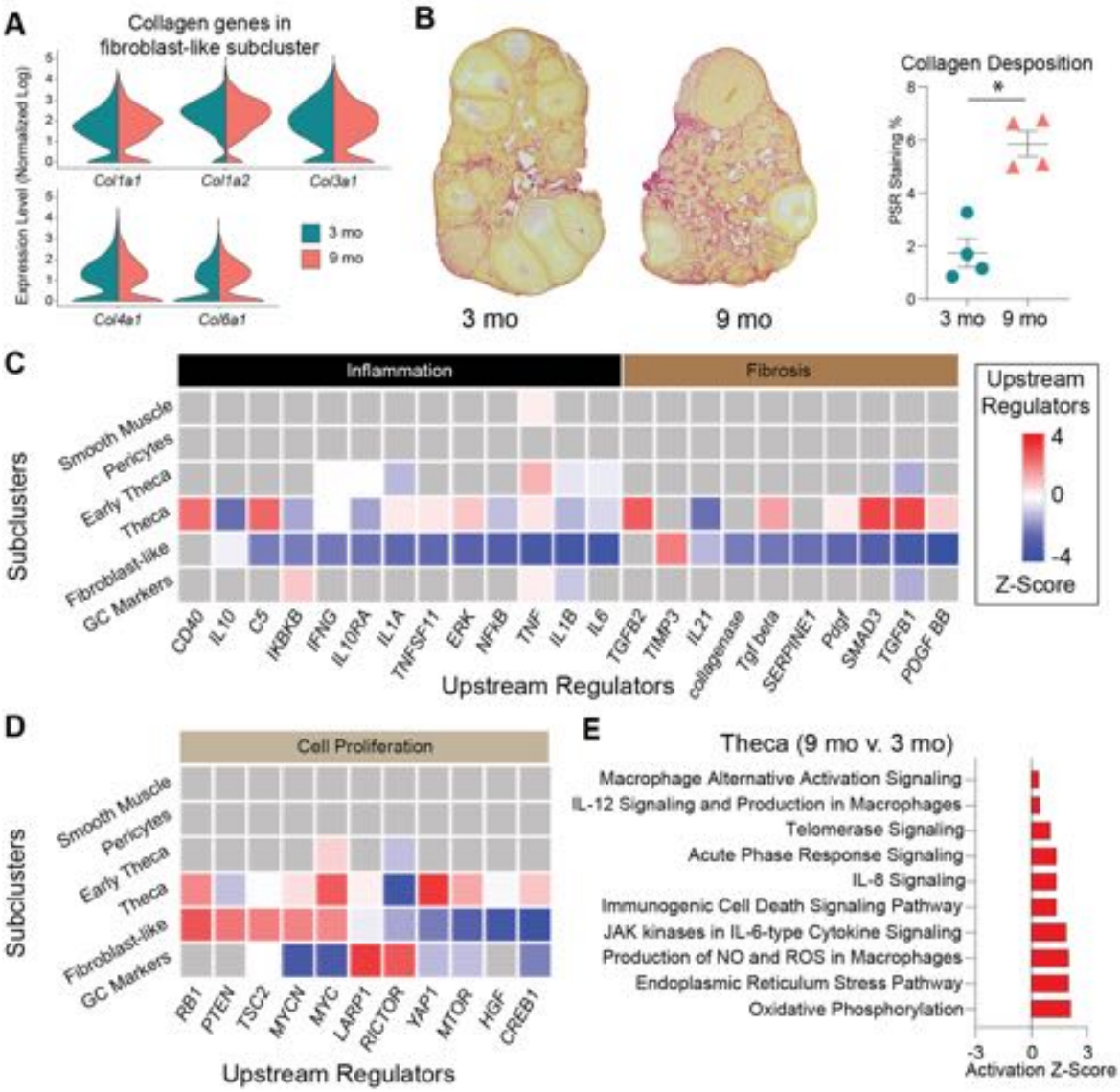

Fig 5: Biological significance of altered pathways in ovarian stroma and theca SCLs. (A) Expression of collagen genes in the fibroblast-like stroma cluster does not change with age. (B) PSR staining of collagen deposition in 3- and 9-month-old ovaries. Quantitation of PSR % staining is presented as mean ± SEM. * represents statistical difference ($p<0.05$) by one-tailed t test.(C-D) IPA upstream regulator analyses of age-related changes in stroma and theca SCLs (9 months vs. 3 months, z-score).

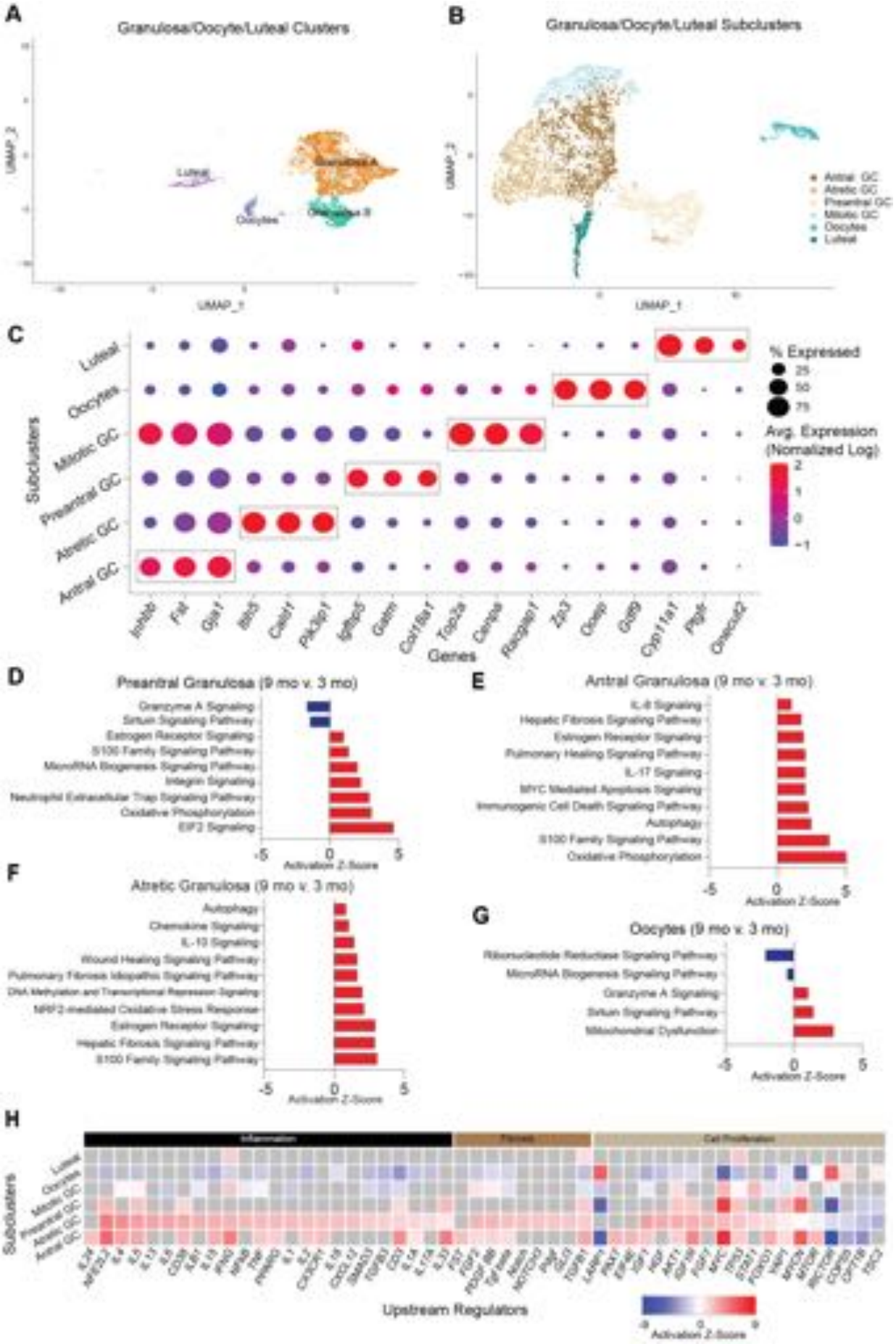

Fig. 6: Sub-clustering of granulosa cells, oocytes and luteal cells. (A) UMAP of granulosa, oocytes and luteal cells CLs used for sub-clustering (B) UMAP of granulosa/oocytes/luteal SCLs. (C) Dot plot of markers used for SCL cell-type identification. (D-G) Z-scores indicating activation or inhibition of pathways during aging by IPA analysis in (D) preantral granulosa cells, (E) antral granulosa cells(F) atretic granulosa cells, and (G) oocytes. (H) Z-scores indicating activation or inhibition of upstream regulators with aging by IPA analysis in granulosa/oocytes/luteal SCLs.

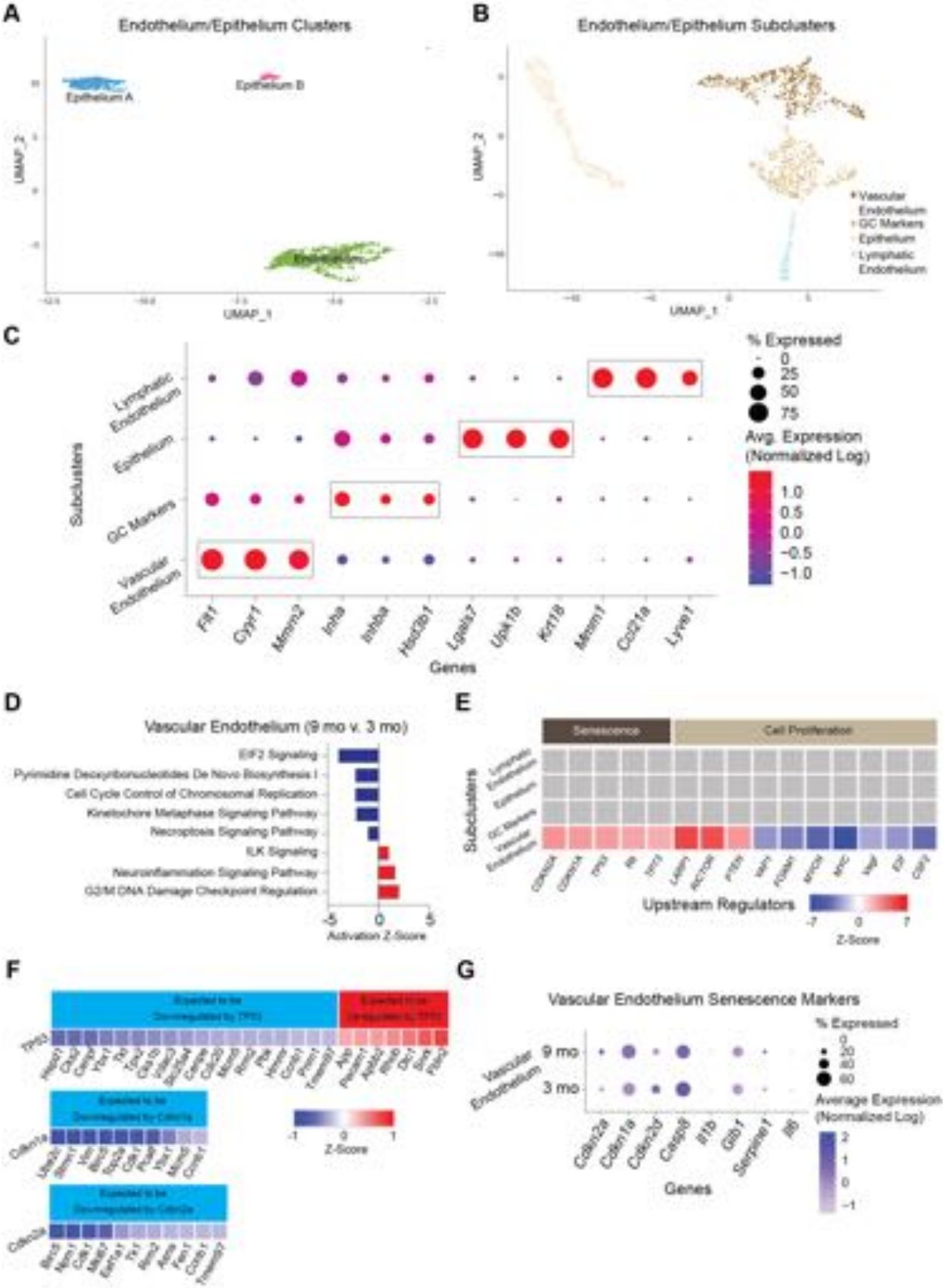

Fig. 7: Sub-clustering of endothelial and epithelial cells. (A) UMAP of endothelium and epithelium CLs used for sub-clustering. (B) UMAP of endothelium/epithelium SCLs. (C) Dot plot of markers used for SCL cell-type identification. (D) Z-scores indicating activation or inhibition of pathways altered with aging by IPA analysis in vascular endothelial cells. (E) Z-scores indicating activation or inhibition of upstream regulators during aging by IPA analysis in endothelium/epithelium SCLs. (F) Z-scores indicating up or downregulation of genes by TP35,

Cdkn1a and Cdkn2a genes. (G) Dot plot of expression of cell senescence markers in vascular endothelial cells in 3- and 9-month-old ovaries.